Variational study of vacancies in solid ^{4}He with shadow wave functions

F. Pederiva
Laboratorio di Fisica Computazionale, Dipartimento di Fisica and INFM, Universitá di Trento, Via Sommarive, 14, I-38050 Povo, Trento, Italy;
Cornell Theory Center, Cornell University, Ithaca, New York 14853;
and Laboratory of Atomic and Solid State Physics, Cornell University, Ithaca, New York 14853

G. V. Chester
Laboratory of Atomic and Solid State Physics, Cornell University, Ithaca, New York 14853

S. Fantoni
S.I.S.S.A., International School of Advanced Studies, via Beirut 2/4, I-34014 Trieste, Italy

L. Reatto
INFM and Dipartimento di Fisica, Universitá di Milano, via Celoria 16, I-20133 Milano, Italy
(Received 17 March 1997)

We employ the shadow wave function (SWF) formalism to obtain estimates of the energy of formation of a vacancy in hcp, fcc, and bcc ^{4}He crystal at $T=0$ K. We find that this energy is a strong function of density, in agreement with experiment. The use of a more efficient sampling with a smart Monte Carlo technique, allowed us to observe the motion of the vacancy through the crystal. We also present data on the occupation of the Wigner-Seitz cells. The occupation of the cells changes along the run, showing the mobility of the particles and of the vacancy. As a byproduct of this study we present results for the energy of perfect hcp and bcc crystals described by a SWF. [S0163-1829(97)09134-0]

I. INTRODUCTION

A quantum crystal, such as solid ^{4}He, differs from a normal solid in that the atoms execute very large amplitude vibrations about their lattice sites. As a consequence the kinetic energy of the crystal is comparable to the potential energy. In a normal crystal, at low temperature, the kinetic energy is typically only a few percent of the potential energy. The properties of impurities and vacancies in a quantum crystal are also strikingly different. The large amplitude motion leads to a different picture of these entities, both become delocalized and can travel through the crystal.[1] The experiments to measure the energy of formation are unfortunately in conflict with one another. This data has recently been carefully reviewed by Burns and Goodkind.[2] An earlier review was given by Fraas, Granfurs, and Simmons.[3] The main focus of this paper is a calculation of the energy of formation of a vacancy in solid helium four. We have chosen to compare our results with those obtained by x-ray measurements[3] of the change in lattice parameter with temperature. The values obtained in this way for the formation energy are generally lower than those found in other experiments. While these experiments are not unambiguous in their interpretation[2] they appear to be less so than others which also show the presence of thermally activated defects.

There have been several theoretical studies of vacancies in solid helium. It is possible to account for the main features of delocalization using semiphenomenological models.[4] A recent paper[5] provides a description of the motion of vacancies based on a lattice-gas model. The static properties of a vacancy in a quantum crystal can be described using the Lekner-Feynman approach.[6] This calculation shows how important it is to include the delocalization effects if one is to reproduce the correct density dependence of the formation energy. Recent work by Stillinger and Hodgdon[7] obtained an estimate of the vacancy concentration at absolute zero. This subject, which has received considerable theoretical attention,[1,8–10] is however outside the scope of this work. The estimate was based on a Jastrow model wave function which provides a ''classical'' description of solid helium. In particular, near melting the zero-point motion described by this wave function has the Lindeman value, which is much smaller than that found in solid helium. The theoretical work which is closest to our own was carried out by Hetherington.[11] Using the well-known Nosanow-Jastrow wave function he estimated both the formation energy of a static vacancy and the band structure of a delocalized vacancy in solid ^{3}He. This work was limited by the structure of the wave function that was used. A Nosanow-Jastrow function will always tend to produce a very localized picture of a vacancy. This is because the atoms in the solid are placed in Gaussian orbitals on predetermined lattice sites with only a small overlap of the orbitals. We believe that it is essential to use a wave function to describe the solid in which the atoms are free to relax in the neighborhood of the vacancy and in which delocalization can occur.

The energy of formation of a single vacancy in a system of N particles and N_l lattice sites with a density $\rho=N/V$ can be defined as

$$\Delta E_{\rm vac}=E(V',\ N-1,\ N_l=N)-\frac{N-1}{N}E(V,N,N_l=N), \tag{1}$$

where $V'=V[(N-1)/N]$. The formation energy $\Delta E_{\rm vac}$ can be represented as a sum of terms due to the energy of a static vacancy, to the lattice distortion around the defect and to the tunneling of atoms in the crystal.[4,11] There is no reason to expect that any of these contributions is small in a highly quantum crystal such as low-density solid ^{4}He. This observation places stringent requirements on any microscopic theory of vacancies in ^{4}He. The shadow wave function[12,13] (SWF) formalism has, we believe, the necessary flexibility to describe this system. The main feature of a SWF is that it allows for a spontaneous symmetry breaking when the density is above the melting point of the solid.[14] As a consequence there is no need to impose an *a priori* crystal structure on the system, particles can exchange positions, and the lattice structure can relax around the defect. Thus the SWF is a suitable trial wave function for variational Monte Carlo (VMC) calculations to study the energy of formation, possible modifications in the local structure, and the delocalization of vacancies. If we used a Nosanow-Jastrow wave function, which localizes the particles in Gaussian orbitals centered on predetermined lattice sites, then the necessary flexibility in the wave function is no longer present. A vacancy, modeled using this wave function, is basically a model of a static vacancy. We will compare the results of our simulations with those based on the Nosanow-Jastrow function.

Our variational calculation is likely to converge rather slowly due to slow structural relaxation processes. Moreover the energy of a vacancy must be evaluated as a difference between two large numbers. Thus such calculations are very demanding, and require improved sampling methods in conjunction with the use of large parallel machines. In this paper we present in Sec. II a review of the SWF method, in Sec. III a description of the technical procedures used in the simulation, in Sec. IV the results of simulations performed with 108/107 and 256/255 particles in a face-centered-cubic lattice, and 180/179 particles in an hexagonal-close-packed lattice. An estimate of the vacancy formation energy in the body-centered-cubic lattice is also presented. Section V is devoted to conclusions.

II. SHADOW WAVE FUNCTIONS

The shadow wave function[12,13] for a system of N ^{4}He atoms can be written in the form

$$\Psi(R)=\int dS K(R,S)\psi_S(S), \tag{2}$$

where $R=\mathbf{r}_1\ldots\mathbf{r}_N$ are the coordinates of the atoms and $S=\mathbf{s}_1\ldots\mathbf{s}_N$ is a set of auxiliary (''shadow'') variables. The function $\psi_S(S)$ is a many-body function for the shadows, while $K(R,S)$ is the product of a many-body function for the atoms $\psi_R(R)$ and of a term $\theta(R,S)$, which correlates real and shadow degrees of freedom:

$$K(R,S)=\psi_R(R)\,\theta(R,S). \tag{3}$$

The integration over the shadow variables in Eq. (2) introduces in $\Psi(R)$, in an implicit way, correlations between the helium atoms at every order. In the VMC method one computes the average value of the Hamiltonian operator $\hat{H}$ with the trial wave function Ψ

$$E_T=\frac{\langle\Psi|\hat{H}\Psi\rangle}{\langle\Psi|\Psi\rangle},\quad \hat{H}=-\frac{\hbar^2}{2m_4}\sum_{i=1}^{N}\nabla_i^2+\sum_{i<j}v(r_{ij}), \tag{4}$$

and minimizes E_T with respect to the parameters entering the wave function. The inter-atomic potential $v(r)$ for ^{4}He can be accurately represented by the Aziz potential.[15] As we have already mentioned an important feature of the SWF is that it provides a stable crystalline phase without imposing one-body localizing factors at assumed equilibrium positions; localization arises as the result of the implicitly introduced many-body correlations. The functions ψ_α, $\alpha=R,S$ and $\theta(R,S)$ have the following forms:

$$\psi_R(R)=\exp\left(-\frac{1}{2}\sum_{i<j}u_{pp}(r_{ij})\right),$$

$$\psi_S(S)=\exp\left(-\sum_{i<j}u_{ss}(s_{ij})\right),$$

$$\theta(R,S)=\exp\left(-\sum_{i=1}^{N}u_{ps}(|\mathbf{r}_i-\mathbf{s}_i|)\right). \tag{5}$$

We parametrize the correlation pseudopotentials $u_{\alpha\beta}$ as in Ref. 16:

$$u_{rr}(r)=\left(\frac{b}{r}\right)^5,$$

$$u_{ss}(r)=\delta v(\alpha r),$$

$$u_{ps}(r)=Cr^2, \tag{6}$$

where b,δ,α,C are variational parameters and v is the interatomic Aziz potential. These functional forms provide good results for the equation of state over a wide range of densities.[16] They give the same equilibrium density as found in Green's function Monte Carlo (GFMC) calculations, $\rho=0.021\,86$ Å^{-3}, an energy 10% off the experimental value. The melting and freezing densities reproduce the values of GFMC calculations.[17] ($\rho_f=0.026\,23$ Å^{-3} and $\rho_m=0.029\,40$ Å^{-3}, respectively), and above the melting density, a stable solid phase is found. In Table I we report the optimal values for the variational parameters at the four values of density of the solid we considered. For three of these densities we can make accurate comparisons with the exist-

TABLE I. Optimal values of variational parameters appearing in the SWF at the densities considered in this work. For the definition of the parameters see text. In the table are reported also the values of the side σ of the fcc elementary cubic cell, and $a=2.556$ Å.

ρ (Å)$^{-3}$	b/σ	$C\sigma^2$	δ (K^{-1})	α	a/σ
0.02898	1.080	5.7	0.11	0.870	2.021
0.02919	1.080	5.7	0.11	0.870	2.017
0.02940	1.080	5.7	0.11	0.875	2.012
0.03294	1.095	5.9	0.10	0.890	1.937

ing experimental data. However we note that the two lowest densities are below the melting density of our crystals, as determined by a double tangent construction. Both of these densities are however above the experimental melting density. We know from previous simulations that at these densities the solid is stable over very long runs. For this reason we think it reasonable to carry out vacancy calculations even though we are below the thermodynamic melting point of our crystal.

III. SIMULATION METHODS AND SAMPLING

In writing Eq. (1) we have assumed that we have a wave function which can describe a crystal with one vacancy. In a wave function with localization factors this can be easily achieved, because the remaining $N-1$ particles are localized in the neighborhood of lattice sites. It is less obvious that a SWF can provide such a description. The fact that localization of the particles derives from high-order correlations does not guarantee that when we start the system from a configuration corresponding to a solid in which one particle has been taken out, the system will not evolve toward some disordered state. If N is very large, this may be a real danger, but the use of a relatively small system, (a few hundred particles) with periodic boundary conditions should favor the stability of a defective crystal which fits the simulation cell. We have monitored the stability of our crystal in two ways. First by very careful measurements of the occupancy of the Wigner-Seitz cells. Second by computing the structure function at a reciprocal-lattice vector. Both methods show very convincingly that our crystal with one vacancy is stable over long Monte Carlo runs. Thus our shadow wave function not only describes a perfect crystal but can also describe a crystal with point defects. It is worth pointing out that the concentration of vacancies in our simulations is large; up to 1%.

The simulation of a quantum crystal with a vacancy does not present, in principle, any additional difficulty in comparison with simulating a perfect lattice. Nevertheless one has to face two important problems. First of all, the estimate of the energy of the vacancy can be obtained only as the difference of the total energy in two different simulations [see Eq. (1)], one with N and one with $N-1$ particles, where N is the number of particles needed to fit the lattice in the simulation box. This difference is of relative order $1/N$, and therefore increasing the number of particles, one needs to increase the accuracy in the energy estimation, and, consequently, the computer time needed for the calculations. On the other hand, the number of particles cannot be made too small. In a small system there can be finite-size effects due both to the incorrect treatment of the tail of the potential energy and to the possible interaction of the vacancy with its periodic images. Due to the periodic boundary conditions the vacancy in our simulation cell is a member of a periodic array of vacancies. It is therefore especially important to minimize any effects from this periodic array by simulating large enough systems.

The second problem arises from the slow convergence of the computation due to fairly rare events corresponding to atoms leaving their original lattice site to occupy a vacant site. In order to improve the convergence we can use a different way to generate the random walk in configuration space. The average value of a local operator $\hat{O}(R)$ with the SWF is evaluated by computing an integral of the form:

$$\int\int\int dR\,dS\,dS'\,\pi(R,S,S')\hat{O}(R), \tag{7}$$

where

$$\pi(R,S,S')=\psi_R^2(R)K(R,S)K(R,S')\psi_S(S)\psi_S(S')/\mathcal{N}, \tag{8}$$

and $\mathcal{N}$ is a normalization such that $\int dR|\Psi(R)|^2=1$. The function $\pi(R,S,S')$ is the probability distribution for all the real and shadow degrees of freedom entering the calculation. In all previous work with the SWF this probability was sampled by means of a Metropolis algorithm, moving particles and the two sets of shadows sequentially. However, looking at the structure of the probability distribution π one can see that due to the form of the kernel K, the system can be viewed[13] as being composed of ''trimers,'' each formed by a particle and by two shadows. The harmonic force connecting particles and shadows makes it very difficult to break the trimer, and if one moves the three components separately, the possibility of leaving the original lattice site is small. In order to increase the efficiency of the sampling we have used collective moves of the trimers. This is however only effective if we increase efficiency of the moves by introducing a pseudoforce, in the way that is often used in classical simulations.[18] We give details of this ''smart Monte Carlo'' in the Appendix.

For a given density, $\rho=N/V$, simulations were performed in pairs, one with N particles at volume V and one with $N-1$ particles at volume $V'=V[(N-1)/N]$. The density of the two systems is thus the same. For the fcc crystal we used $3\times3\times3$ elementary cubic cells accommodating $N=108$ particles. With this system we performed four pairs of simulations at four different values of the average density ρ (see Table II). In order to check size dependence we performed a pair of simulations at a density $\rho=0.0294$ Å^{-3} with $N=256$ particles, corresponding to $4\times4\times4$ elementary cells of the fcc lattice. For the hcp lattice, the equilibrium phase for solid ^{4}He for at low temperatures, we performed four pairs of simulations, at the same densities of the fcc crystal, with $N=180$ particles, corresponding to $5\times3\times3$ elementary cells, in an hcp lattice. The length of each run was 10^6 Monte Carlo steps (MCS), where a MCS is defined as a complete sweep of trial moves over all the trimers in the system. Finally, we estimated the vacancy formation energy

TABLE II. Estimated energy per particle and formation energy of a vacancy in fcc, hcp, and bcc ^{4}He at $T=0$ K.

ρ (Å^{-3})	N	Lattice	$\epsilon(N-1)$ (K)	$\epsilon(N)$ (K)	$\Delta E_{\rm vac}$ (K)
0.02898	108	fcc	−4.931(16)	−5.089(16)	16.3±1.5
0.02898	180	hcp	−5.082(15)	−5.147(15)	11.6±2.0
0.02919	108	fcc	−4.924(16)	−5.102(15)	19.0±2.0
0.02919	180	hcp	−5.027(15)	−5.105(15)	13.9±2.0
0.02940	54	bcc	−4.640(30)	−5.026(30)	20.8±2.5
0.02940	108	fcc	−4.900(15)	−5.079(15)	19.1±1.5
0.02940	180	hcp	−5.025(15)	−5.107(15)	14.7±2.0
0.03294	108	fcc	−3.276(16)	−3.630(16)	37.9±1.6
0.03294	180	hcp	−3.443(15)	−3.633(15)	34.0±2.0

in the bcc phase at density $\rho = 0.0294$ Å^{-3}, with a pair of runs of 2×10^6 MCS, with $N=54$, corresponding to $3\times3\times3$ elementary cubic cells. For this lattice structure we did not carry out a search for the best set of parameters, corresponding to the lowest energy. We merely fixed three of the parameters b, δ, α, at the values found for the fcc and hcp crystals. The Gaussian coupling constant C was, however, decreased from $5.7\sigma^{-2}$ to $5.0\sigma^{-2}$. Unless this is done the bcc crystal is unstable at the lowest densities. Our aim in the bcc crystal was to establish that it is stable in our simulations both with and without a vacancy. Since the system size, 54 particles, is small and the wave function has not been optimized it is rather likely that the formation energy we report can be improved. In order to keep the centers of vibration for the atoms fixed we use a frame of reference with the origin at the center of mass of the system which is recomputed for each configuration generated in the random walk.

IV. RESULTS

For the three highest densities, the energies of the hcp and fcc crystals are very close, within the statistical noise of our simulations. Only at the lowest density, $\rho = 0.028\,98$ Å^{-3}, the hcp result is significatively below the fcc. The bcc solid is less bound than either the fcc and the hcp, as might be expected. From our simulations we extracted information on the formation energy of the vacancy as function of the density, the crystal structure and the number of particles in the simulation box. In Table II we report the values of the energy per particle as a function of the density for the different lattices for a perfect crystal and for a crystal with a vacancy, together with the estimate $\Delta E_{\rm vac}$ of the formation energy. Expressed in terms of $\rho = N/V = N - 1/V'$, $\Delta E_{\rm vac}$, Eq. (1), becomes

$$\Delta E_{\rm vac} = [\,\epsilon(N-1,\rho,N_l=N) - \epsilon(N,\rho,N_l=N)\,](N-1), \tag{9}$$

where ϵ is the energy per particle. It should be noted that the thermodynamic limit of $\Delta E_{\rm vac}$ in Eq. (9) corresponds to the vacancy formation energy in the limit of zero vacancy concentration. For this reason it is important to study the behavior of $\Delta E_{\rm vac}$ as function of N. We performed runs with $N=256$ atoms at density $\rho = 0.029\,40$ Å^{-3}, with the results $\epsilon(256) = -5.043 \pm 0.015$ K and $\epsilon(255) = -4.970 \pm 0.015$ K. This gives $\Delta E_{\rm vac} = 18.61 \pm 5.3$ K, which agrees within the error bars with the value obtained with $N=108$. This enables us to assume that our results are a good representation of the thermodynamic limit. The lattice structure does have an influence on the value of the vacancy formation energy. In the hcp phase $\Delta E_{\rm vac}$ is about 4 K lower than in the fcc phase. In all cases, the formation energy of the vacancy is strongly dependent on the density, in good qualitative agreement with present experiments.[3] Our results are summarized in Fig. 1. From Table II we see that $\Delta E_{\rm vac}$ for the bcc crystal is very close to that of the fcc lattice. As we have mentioned the vacancy energy in this structure is subject to larger uncertainties due to the small system size and unoptimized wave function. Its value ($\sim$21 K) is larger than the experimental value[3] ($\sim$10 K) for bcc ^{4}He. Again we note that the experimental value is subject to fairly large uncertainties due to the choice of vacancy model used to interpret the data.

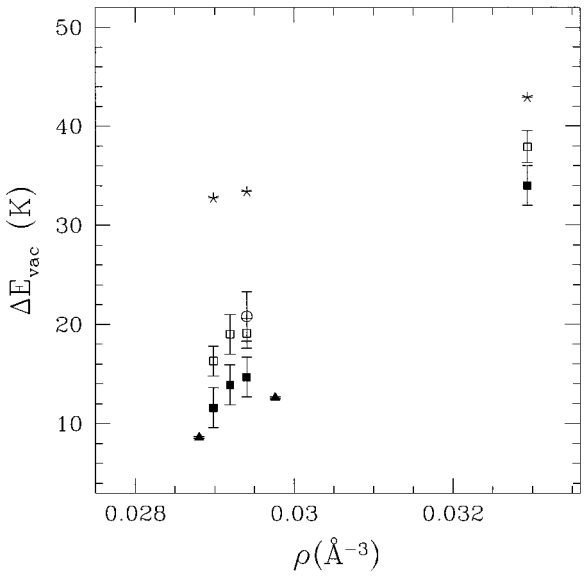

FIG. 1. Vacancy formation energy $\Delta E_{\rm vac}$ vs reduced density. Solid triangles: data from Ref. 3, open squares: variational estimates for the fcc phase; filled squares: for the hcp phase; open circle: for the bcc phase. Stars: formation energy of a static vacancy [see Eq. (10) in text].

Our formation energies have rather large statistical uncertainties. These arise because, as we have pointed out, we are doing a ''$1/N$'' calculation. We can of course reduce these statistical uncertainties by performing longer MC runs. However the uncertainties we report are of the same magnitude as those in the experimental results. Before carrying out much longer MC simulations we need to carefully investigate how sensitive are our results to system size, type of shadow wave function, and two-body potential.

In Table III we compare the estimated energy for a static vacancy at density ρ, which is given by

$$\Delta E_{\rm vac}^{\rm st} = -\frac{\langle V\rangle}{N} + Pv, \tag{10}$$

where $\langle V\rangle$ is the average value of the potential energy in the sample, $v = 1/\rho$ is the specific volume, and P is the pressure of the system. The difference between $\Delta E_{\rm vac}$ and $\Delta E_{\rm vac}^{\rm st}$ is a measure of the contributions due to the lattice relaxation and to the motion of the vacancy through the crystal. The difference between the static energy and the SWF estimate strongly depends on the density. At density $\rho = 0.032\,94$ Å^{-3} the nonstatic effects appear to be much less important than close to the melting point. This is due to the fact, discussed below, that the mobility of the vacancy is

TABLE III. Energy of the static vacancy $\Delta E_{\rm vac}^{\rm st}$ vs VMC result for the fcc lattice. The difference is due to lattice relaxation and tunneling.

ρ (Å^{-3})	$\Delta E_{\rm vac}^{\rm st}$ (K)	$\Delta E_{\rm vac}$ (K)
0.02898	38.3	14.3 ± 1.5
0.02940	38.5	19.1 ± 1.5
0.03294	46.5	37.9 ± 1.6

quite strongly depressed at the higher density. At the lower densities, the energy is not only reduced by about 50% with respect to the static case, but it shows a much stronger density dependence. This means that at low density the dynamic effects are as important as the static effects.

We can obtain information both on lattice relaxations and on the vacancy mobility by analyzing the configurations generated in the simulations. The deformation of the lattice can be studied by looking at the distribution of the particles near the vacancy. This can be done dividing the sample into Wigner-Seitz (WS) cells. We have performed this analysis only in the fcc lattice. Each WS cell is centered on the sites of the original lattice, and the boundaries are given by the 12 planes:

$$(\pm x \pm y) = \frac{a}{2}; \quad (\pm x \pm z) = \frac{a}{2}; \quad (\pm y \pm z) = \frac{a}{2}. \quad (11)$$

The coordinates refer to the center of mass of the system. We find that the particles in a perfect crystal nearly always occupy the same cell during the simulation. However, due to the large quantum fluctuations, the atoms occasionally visit the neighboring cells, creating vacant and doubly occupied WS cells. In a long run we find that close to 1% of the WS cells in the perfect crystal are unoccupied with a nearest-neighbor (NN) cell doubly occupied. We call these fluctuations pseudointerstitial-vacancy (PIV) pairs. We computed the following quantities:

$$\rho^F_{\mathrm{NN}}(r) = \left\langle \frac{1}{N_{\mathrm{NN}} N_F} \sum_{i(F)} \sum_{\langle j \rangle_i} \delta(|\mathbf{r} - \mathbf{r}_j + \mathbf{R}_i|) \right\rangle, \quad (12)$$

$$\rho^F_{\mathrm{NN}}(r) = \left\langle \frac{1}{N_{\mathrm{NN}} N_E} \sum_{i(E)} \sum_{\langle j \rangle_i} \delta(|\mathbf{r} - \mathbf{r}_j + \mathbf{R}_i|) \right\rangle, \quad (13)$$

where N_E and N_F are the number of empty and of singly occupied WS cells in a given configuration, N_{NN} is the number of nearest neighbors, $\mathbf{R_i}$ are the coordinates of the lattice site i, and $\mathbf{r_j}$ are the coordinates of particle j. The sum over $\langle j \rangle_i$ is extended over the particles in the cells which are nearest neighbors to cell i. The sum on $i(F)$ is only extended to all singly occupied cells, while the sum on $i(E)$ is extended to the empty cells which do not have a doubly occupied cell as nearest neighbor. This is done in order to remove the contributions from PIV pairs, which are present for 1% of the cells for both the systems with N and $N-1$ atoms. The quantities (12) and (13) give direct information on the distortion both in terms of the shifting of the equilibrium positions and of the density distribution. In Fig. 2 we plot ρ^E_{NN} and ρ^F_{NN} computed with 947 equally spaced configurations out of 9.47×10^5 at density $\rho = 0.029\,40$ Å^{-3} with 255 particles. As it can be seen the distribution of the nearest neighbors of a vacancy is both broadened and becomes asymmetric when compared to that of a filled site. The following construction allows one to see this distortion more clearly. We note that the right-hand side of the distribution can be very accurately fitted to a Gaussian. This is shown as the dashed curve in the figure. When we plot this complete Gaussian we immediately see that a large tail emerges, above the Gaussian, on the side near the vacancy. Clearly the near neighbors have moved in, slightly, towards the vacancy. The center of this Gaussian has also shifted inward with respect to the distribution for the perfect crystal.

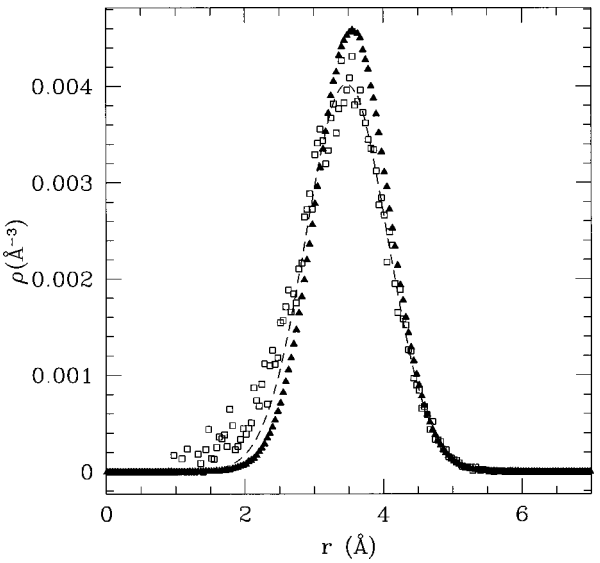

FIG. 2. Nearest-neighbor density around a lattice site. Triangles: density around sites in a perfect crystal. Empty squares: density around empty sites in a crystal with one vacancy. Dashed line: Gaussian fit of the outer part of the density around empty sites. The data for the vacancy are for $N = 255$ particles in an fcc lattice at density $\rho = 0.029\,40$ Å^{-3}.

We can also use our configurations to study the motion of the vacancy, and its influence on the motion of the particles. While we are able to analyze the configurations generated from our MC simulations to show unambiguously that the vacancy is mobile we need to caution the reader that one cannot literally interpret the motion in terms of a trajectory. We demonstrate the motion by computing various well-defined expectation values, such as the occupancy of the WS cells. However since there is no real ''time'' variable in our simulations we cannot immediately think of trajectories or extract a diffusion constant. In Fig. 3 we show the one-body density of shadows $\rho_s(r)$ with respect to their initial positions for the system with $N = 255$ particles at average density $\rho = 0.029\,40$ Å^{-3}. The density profile of the particles is similar to that of the shadows, the latter being more resolved due to the stronger localization of the shadows. The profile is split in two parts: on the left we show the density inside the sphere of radius equal to half of the nearest-neighbor distance, on the right the density outside, on a larger scale. The peak in the outer region means that a fraction of the particles have left their original lattice sites to reach a new equilibrium position. With $N = 256$ the outer peak is not present, this shows that no such displacements are present for the full lattice. We should note that this effect is due to the finite length of the simulation. In the real system, and also in the system described by the SWF, the particles exchange positions, and if one could measure the true density profile around a given site, one should see the particles equally distributed over all the sites in the lattice. However in the simulation of the perfect crystal spontaneous exchange of particles occurs so rarely that we do not observe it. When a vacancy is present the mobility is highly affected, and with efficient sampling we start to observe such events. The jump

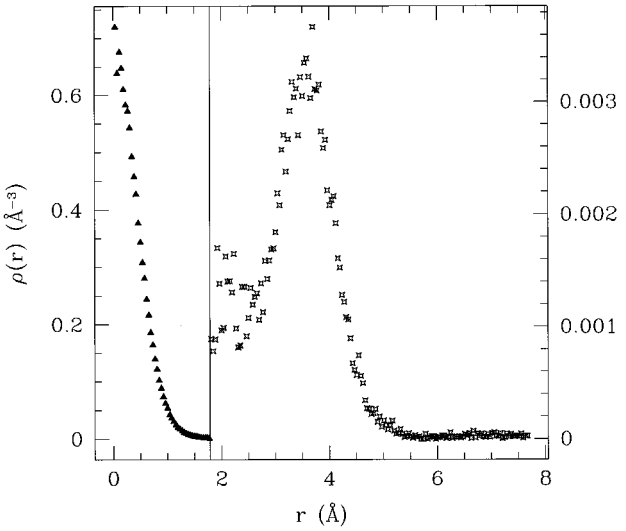

FIG. 3. One-body density profile for shadows around a lattice site in a crystal with one vacancy. In the left part of the figure we show the density inside a sphere of radius equal to half of the NN distance; on the right (on a larger scale) we show the density outside this sphere. Results are for $N=255$ particles at $\rho=0.029\,40$ Å^{-3}.

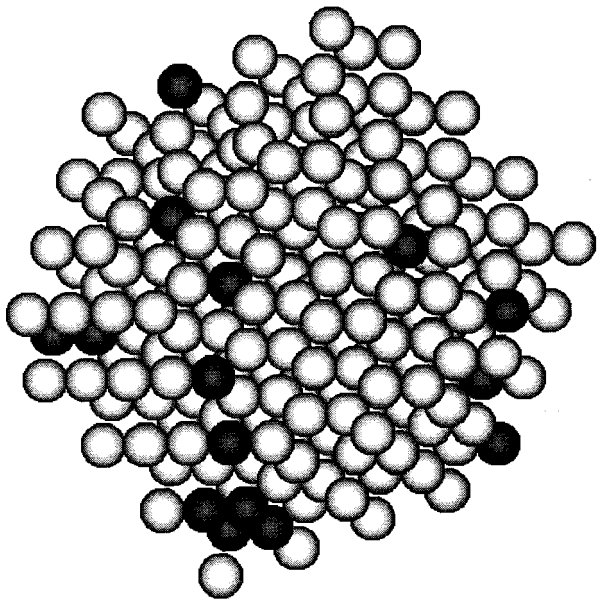

FIG. 5. The black cells are Wigner-Seitz cells which were unoccupied at some time during the run. The grey cells are these that were occupied throughout the run. The run consisted of 10^6 sweeps.

of particles between different lattice sites can be observed also from a direct analysis of the configurations. In Fig. 4 we have plotted the projection of 400 equally spaced configurations, out of 4×10^5, on the x-y plane. The dark triangles represent the positions for one specific particle. It can be seen that at least three different sites are occupied by the particle. We observe such motions only in a definite region of our simulation box, and from that we can argue that the mobile particles are those close to the vacancy. No such jumps of particles are observed in the perfect crystal during our longest MC runs.

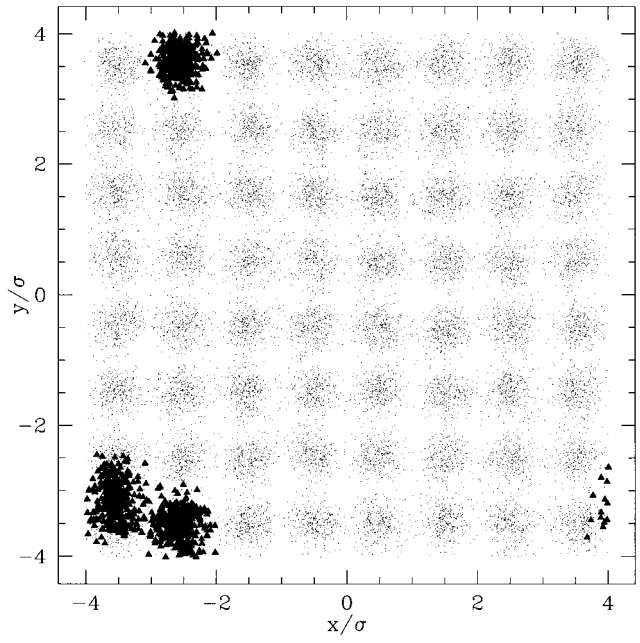

FIG. 4. Projection on the x-y plane of 400 equally spaced configurations out of 4×10^5 for $N=255$ at $\rho=0.029\,40$ Å^{-3}. The triangles represents the positions of one given particle in the box (see text).

In Fig. 5 we show the motion of the vacancy. The grey cells are Wigner-Seitz cells which were occupied throughout a run of 10^6 sweeps. The black cells are Wigner-Seitz cells which at some time were empty during the run. To make this plot we ignored all empty cells which also had a doubly occupied NN cell. That is to say we ignored all PIV pairs. It is clear from this figure that the vacancy moves over large distances. In a much longer run it would presumably move through the entire simulation cell. We can also observe the motion of the vacancy by determining the distribution of empty cells in the simulation box. In Fig. 6 we show a histogram of the number of times a given WS cell in the simulation box is found empty (computed from 974 equally spaced configurations out of 9.74×10^5). In the upper graph we plot the result for $N=256$, which has to be compared with the lower graph obtained with $N=255$ (note the change of scale). We can see that the average number of counts is very different in the two cases. For the perfect crystal, vacant WS cells are due to the PIV pairs. There are however no cells which are unoccupied more than 25 times in the run. However, when a vacancy is present, one observes the presence of much higher peaks. In this run there are 17 cells which were empty 40 or more times. We can reasonably assume that these higher peaks represent positions of the vacancy. This is again direct evidence that the vacancy occupies many different positions in the crystal. In Fig. 7 we show the same plots, as in Fig. 6, but now for data taken at our highest density, $\rho=0.0324$ Å^{-3}. There is a striking difference between the data at this density and the data at the lower density. Comparatively few cells are frequently unoccupied and one single cell is unoccupied most of the time. Clearly at the higher density the vacancy is comparatively

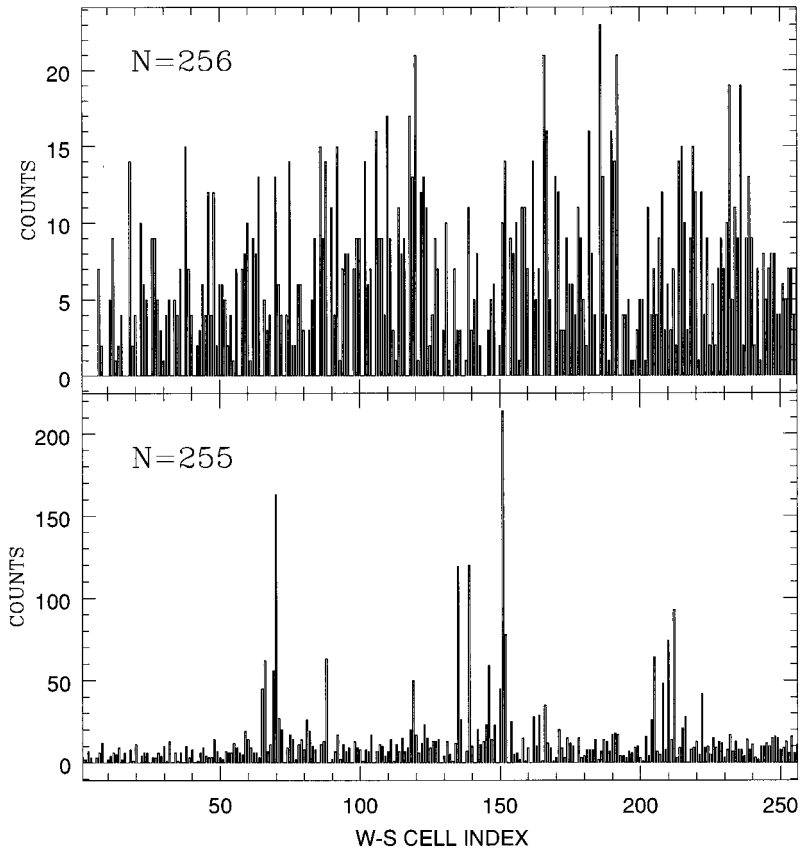

FIG. 6. Histogram of counts of occurrence of an empty cell. Abscissas are cell indexes. Upper part: perfect crystal; lower part: crystal with vacancy. The data are from 974 equally spaced configurations in a run of 9.74×10^5 sweeps; no cell is unoccupied more than 25 times in the perfect crystal. In the crystal with a single vacancy there are 17 cells unoccupied at least 40 times.

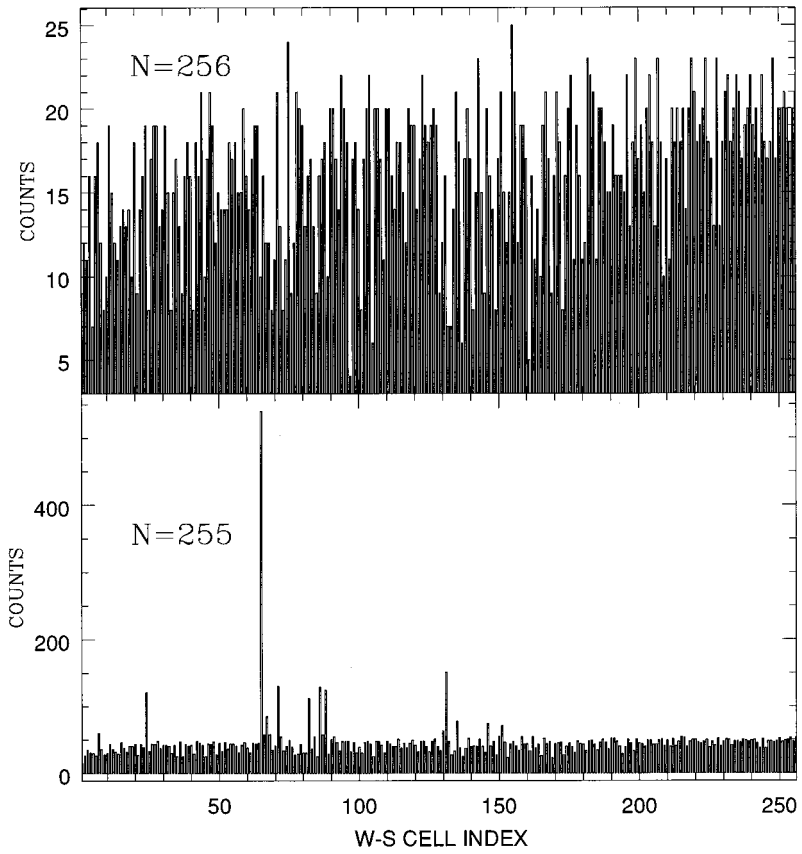

FIG. 7. Same data as in Fig. 6 but now taken at the highest density $\rho=0.032\,94\ \text{Å}^{-3}$. Note that there are now a comparatively small number of unoccupied cells when a vacancy is present. At the lower density 17 cells were unoccupied at least 40 times, now there are only seven such cells. Moreover one cell is unoccupied nearly 600 times. Clearly the vacancy is much less mobile.

immobile. This decreased mobility is confirmed by the fact that the energy of formation at this density is much closer to the static energy, see Table III.

V. CONCLUSIONS

In this paper we have presented a calculation of the energy of formation of a vacancy in solid ^{4}He which allows for lattice relaxation and delocalization of the vacancy. The energy is strongly dependent on the density and is in reasonable agreement with the experimental values obtained by Fraas, Granfors, and Simmons.[3] Since our calculation is based on a variational wave function our estimate provides an upper bound to the energy of formation. An important result of our simulation is that the vacancy is mobile; in a moderately long (10^6 MC sweeps) run it occupies many different sites in the lattice. We find however that the mobility is sharply reduced at about 12% above the melting density.

We plan to extend this work in several ways. First, as we have already mentioned, we must investigate how sensitive are our results to system size, type of shadow wave function, and two-body potential. We have already done some system size studies but we believe an even more systematic study is warranted. Once these investigations have been completed we will improve the accuracy of our results with much longer MC runs. Two physically interesting systems can also be simulated without great difficulty. First we can simulate a crystal with a vacancy and a helium three impurity. The interesting question for this system is whether the vacancy and impurity form a ''bound'' state, as has been suggested in the literature.[19] Since we can study the correlation between the vacancy and the impurity we should be able to answer this question. Next we can also study a system with two or more vacancies, and study the correlations between the two vacancies. Returning to the system with a single vacancy we can attempt to measure the change in local kinetic energy due to the presence of the mobile vacancy. If we can do this we can then separate the contributions to the energy of formation from lattice distortions and from tunneling. Finally it will be interesting to extend this work to vacancies in solid helium three. However this can only be done when we have a shadow wave function of the correct symmetry and which can account for the magnetic properties of the solid phase.

ACKNOWLEDGMENTS

We thank M. H. Kalos, S. A. Vitiello, and S. Stringari for useful discussions and contributions to this work and Alex Agranov who carried out the initial phase of this work. Part of this work was carried out on the IBM-SP2 at the Cornell Theory Center which is funded by the National Science Foundation, by New York State, I.B.M., and Cornell University. This work was partially supported by Italian Istituto Nazionale di Fisica della Materia and by the Italian Ministry for University and Scientific Research. F.P. was supported, in part, by the National Science Foundation under Grant No. ASC 9626329. We also thank the hospitality of FORUM-INFM at Scuola Normale Superiore in Pisa where part of this work was carried out.

APPENDIX

The probability distribution sampled in SWF-VMC calculations is defined in Eq. (8). In order to be able to move more than one particle or shadow at a time, and in particular to perform trimeric moves, it is convenient to bias the move along the gradients of the probability distribution.[18] The transition matrix used for generating successive positions m,n of the ith trimer is the following:

$$T_{mn}=\frac{1}{\sqrt{(4\sigma\pi)^3}}\, e^{-(\Delta \mathbf{X}_i^{mn}-\sigma \mathbf{F}_i^m)^2/4\sigma}, \tag{A1}$$

where $\mathbf{X}_i$ is the nine-dimensional vector $\mathbf{X}_i=(\mathbf{r}_i,\mathbf{s}_i,s_i')$ and the pseudoforce $\mathbf{F_i}$ is given by $\mathbf{F_i(X)}=\widetilde{\nabla}_\mathbf{i}\ln\pi(\mathbf{X})$, where $\widetilde{\nabla}=(\nabla_r,\nabla_s,\nabla_{s'})$. The moves are performed according to

$$\Delta \mathbf{X_i^{mn}}=\sigma \mathbf{F_i^m}+\xi_\mathbf{G}, \tag{A2}$$

where ξ_G is taken from a Gaussian distribution of zero mean and variance 2σ. Imposing the detailed balance condition[18]

$$T_{m,n}\pi_n=T_{n,m}\pi_m, \tag{A3}$$

one finds the acceptance-rejection criterion. Typical values for σ in our simulations are 0.1 for particles and 0.07 for shadows, in order to get an acceptance of about one third of the moves.

[1] A. F. Andreev and I. M. Lifschitz, Sov. Phys. JETP **29**, 1107 (1969); A. F. Andreev, *Progress in Low Temperature Physics* (North-Holland, Amsterdam, 1982), Vol. 8.
[2] C. A. Burns and J. M. Goodkind, J. Low Temp. Phys. **93**, 15 (1993).
[3] B. A. Fraas, P. R. Granfors, and R. O. Simmons, Phys. Rev. B **39**, 124 (1989).
[4] R. A. Guyer, J. Low Temp. Phys. **8**, 427 (1972).
[5] D. J. Bukman and J. M. J. van Leeuwen, Phys. Rev. B **49**, 226 (1994).
[6] F. Pederiva, F. Dalfovo, S. Fantoni, L. Reatto, and S. Stringari, Phys. Rev. B **55**, 3122 (1997).
[7] J. A. Hodgdon and F. H. Stillinger, J. Stat. Phys. **78**, 117 (1995).
[8] G. V. Chester, Phys. Rev. A **2**, 256 (1970).
[9] A. J. Leggett, Phys. Rev. Lett. **30**, 1543 (1970).
[10] R. A. Guyer, Phys. Rev. Lett. **26**, 174 (1971).
[11] J. H. Hetherington, Phys. Rev. **176**, 231 (1968).
[12] S. A. Vitiello, K. Runge, and M. H. Kalos, Phys. Rev. Lett. **60**, 1970 (1988).
[13] L. Reatto and G. L. Masserini, Phys. Rev. B **38**, 4516 (1988).
[14] F. Pederiva, A. Ferrante, S. Fantoni, and L. Reatto, Phys. Rev. B **52**, 7564 (1995).
[15] R. A. Aziz, V. P. S. Nain, J. S. Carley, W. L. Taylor, and G. McConville, J. Chem. Phys. **70**, 4330 (1979).

[16] T. McFarland, S. A. Vitiello, L. Reatto, G. V. Chester, and M. H. Kalos, Phys. Rev. B **50**, 13 577 (1994).
[17] M. H. Kalos, M. A. Lee, P. A. Whitlock, and G. V. Chester, Phys. Rev. B **24**, 115 (1981).
[18] M. P. Allen and D. J. Tildesley, *Computer Simulation of Liquids* (Clarendon, Oxford 1987).
[19] E. Polturak, I. Schuster, I. Berent, Y. Carmi, S. Lipson, and B. Chabaud, J. Low Temp. Phys. **101**, 177 (1995).